Aquaculture 495 (2018) 115–129

Contents lists available at ScienceDirect

Aquaculture

journal homepage: www.elsevier.com/locate/aquaculture

A novel approach to assess the hydrodynamic effects of a salmon farm in a Patagonian channel: Coupling between regional ocean modeling and high resolution les simulation

Julio Herrera[a,b], Pablo Cornejo[a,*], Héctor Hito Sepúlveda[c], Osvaldo Artal[c,d], Renato A. Quiñones[b,e]

[a] Department of Mechanical Engineering, Faculty of Engineering, University of Concepción, Edmundo Larenas 219, Concepción, Chile
[b] Interdisciplinary Center for Aquaculture Research (INCAR), University of Concepción, O'Higgins 1695, Concepción, Chile
[c] Geophysics Department, Faculty of Physical and Mathematical Sciences, University of Concepción, Concepción, Chile
[d] Departamento de Medio Ambiente, División de Acuicultura, Instituto de Fomento Pesquero, Balmaceda 252, Puerto Montt, Chile
[e] Department of Oceanography, Faculty of Natural and Oceanographic Sciences, University of Concepción, Casilla160-C, Concepción, Chile

ARTICLE INFO

Keywords:
WMLES
CROCO
CFD
Salmon production
Hydrodynamics
Patagonian fjords

ABSTRACT

The interaction between local hydrodynamics conditions and salmon cages are important in disease transmission and in the transport of waste products generated by aquaculture. We propose a modeling methodology to assess the hydrodynamic effects of a salmon farm in a Patagonian channel. The method is based on the coupling between a Coastal and Regional Ocean COmmunity model (CROCO) and a high resolution Large Eddy Simulation (LES) model. A salmon farm located in the Estero Elefantes Channel (45°39′16.50″S–73°35′59.40″W) was used as a study case. The physical coherence of the results was validated by comparison with field current velocities measured with an Acoustic Doppler Current Profiler (ADCP). The model predictions were capable of reproducing the tendencies of the variation although there were some differences in magnitude. The results showed that the hydrodynamics of the Estero Elefantes Channel is dominated by two circulation modes depending on the current direction in the adjacent Moraleda channel. Both circulation modes are characterized by a highly unstable shear flow composed by turbulent structures that interact with the salmon cages. Therefore it is not possible to select a local control volume with arbitrarily defined inlets, outlets and impermeable walls to evaluate hydrodynamic processes relevant to the salmon farms. The presence of the cages modifies the natural hydrodynamics of the channel, attenuating the intensity of the local velocity magnitude and generating recirculation and retention zones near them. However, their effect is not confined locally because the perturbations introduced by the presence of cages are propagated far from them. The transport of material discharged inside the cages was also analyzed. This information should prove useful both for producers and the aquaculture management authority.

1. Introduction

Chile is the second largest salmon and trout producer in the world after Norway (FAO, 2016). Salmon production in Chile has grown exponentially from US$159 million in exports in 1991 to an export value that exceeded the US$3860 million in 2016 (Central Bank of Chile, 2017). Salmon farms in Chile are located in the channels and fjords of Chilean Patagonia due to their suitable water quality and oxygenation conditions (Tironi et al., 2010). Despite the magnitude of the salmon production in Patagonia, little is known about the potential impacts of implementing fish farming systems on the hydrodynamics and ecosystem functioning of the fjords and channels (Cornejo et al., 2014). In terms of global food supply, aquaculture provided more fish than capture fisheries for the first time in 2014 (FAO, 2016). Production of higher-value species, such as salmon and trout, is projected to grow in the next decade (FAO, 2016). However, salmon cage production has raised concerns regarding its potential impacts on the environment produced, for instance, by antibiotics and pesticides used for preventing and treating fish diseases and by solid organic and nutrients wastes from the farms that could cause degradation of local benthic habitats and could contribute to eutrophication and increased risk of algal blooms (e.g. Findlay and Watling, 1997; Fisheries and Oceans Canada,

* Corresponding author.
E-mail address: pabcornejo@udec.cl (P. Cornejo).

https://doi.org/10.1016/j.aquaculture.2018.05.003
Received 31 May 2017; Received in revised form 16 April 2018; Accepted 1 May 2018
Available online 03 May 2018
0044-8486/

2003; Buschmann et al., 2009, 2012; Wang et al., 2012; Price et al., 2015). Current velocity magnitude and direction is a key factor in determining the exchange of water through the cage, areas over which deposition occurs and also in the re-suspension of material (Venayagamoorthy et al., 2011).

Salmon farms have an effect on the hydrodynamics of local currents, oxygen content inside fish cages, and the swimming behavior of fish (Johansson et al., 2007). Fluid dynamics can be critical in determining the incidence of diseases in salmon farms through their influence on dispersal, transmission and encounter rates between organisms (e.g. Gustafson et al., 2007; Aldrin et al., 2010; Salama and Murray, 2011; Samsing et al., 2015). Thus, farm-induced changes on local hydrodynamic conditions (Cornejo et al., 2014), and oxygen levels (Johansson et al., 2007) must be considered in the design, orientation and distribution of farms.

Sustainable global salmon production requires new technologies to improve cage design for diminishing environmental impacts (Chamberlain and Stucchi, 2007; Føre et al., 2016). Technological advances have facilitated the continuous monitoring of oceanographic variables (e.g. Löfgren et al., 2011; Terray et al., 1999; Larson et al., 2013), which helps to understand the effect of the cages on water circulation (Fredriksson et al., 2007). However this approach is costly and requires long-term sampling effort (Langis, 2015). As a complimentary tool to field measurements, numerical simulation studies (e.g. Finite Element Method; Computational Fluid Dynamics, CFD) can be used to describe physical phenomena and be calibrated and validated with in situ measurements. Numerical simulation studies have allowed to predict scattering of the wastes produced by salmon cage farming (e.g. Gillibrand and Turrell, 1997; Panchang et al., 1997; Doglioli et al., 2004), to study the sanitary barriers that separate them (Olivares et al., 2015), understand the dynamic behavior of the cages under the influence of currents (Bessonneau and Marichal, 1998; Tsukrov et al., 2000; Lee et al., 2008), improve cages design (Fredriksson et al., 2004) and study the effect of the thread and mesh sizes of the cages (Zhao et al., 2007), among others. CFD studies have been oriented mainly to understand the cages effects on local hydrodynamics (Cornejo et al., 2014) as well as the water dynamics inside the cages (Zhao et al., 2013; Bi et al., 2014, 2015), describing explicitly the small-scale fluid dynamic processes through and around a net panel (Patursson et al., 2010). These type of studies cannot be carried out using ocean modeling at a regional scale (e.g. FVCOM, Chen et al., 2003; ROMS, Shchepetkin and McWilliams, 2005) due to the length and time scales for which these regional models were designed. Nevertheless, studies have been performed to attempt to use regional oceanographic models in length scales close to those relevant to salmon cage structures in marine environments (Hasegawa et al., 2011; Chen et al., 2013; Wekerle et al., 2013). The minimum resolution in the computational grids of these studies is of O(kms), which prohibits including salmon cages, which are of O(m).

On the other hand, studies based on Computational Fluid Dynamics (CFD) have been restricted to idealized environments (Cornejo et al., 2014; Winthereig-Rasmussen et al., 2016), without including a coastline, bathymetry, stratification of the water column, winds, etc. A recent study (Winthereig-Rasmussen et al., 2016) investigated the effect of fish farming sea cages in a bay of the Faroe Islands. The authors compared the numerical simulation results to experimental data obtained by ADCP. The velocity deficit found in the simulation overestimated the ADCP data by 50%. However, the control volume employed in the computational model arbitrarily includes wall boundaries in zones where there is no a priori knowledge of current velocities, and inlets and outlets with fixed velocity direction in a zone where the coastline is extremely irregular, which generates turbulent structures that modify the velocity field constantly.

This study investigates the effect of salmon farm cages on the hydrodynamics of a Patagonian channel using a high-resolution LES model and taking its boundary conditions from a regional ocean model.

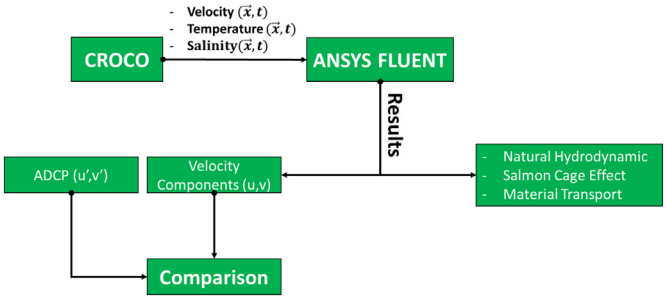

Fig. 1. Flow diagram of the proposed methodology.

The LES model considers a non-idealized environment and boundary conditions located away from the study zone, avoiding an arbitrary definition of a bounded volume control in conditions where an a priori definition is not possible. The physical coherence of the approach is assessed by comparing the numerical model predictions with field current velocities measured with an ADCP located in the vicinity of the salmon cages. This paper is organized as follows. Section 2 describes the theory behind CFD models, the turbulence model used (WMLES), and the representation of salmon cages in the model. Section 3 describes the study area, model geometry, the regional simulation used as boundary condition, and the WMLES simulation. Section 4 presents the results, model comparison with field measurements, and implications for material transport. Finally Section 5 presents the discussion and Section 6 the conclusions.

2. Theory

2.1. Fundamentals

CFD models are a powerful alternative to address geophysical fluid dynamics microscale problems such as the hydrodynamics of salmon farms, where regional oceanographic models are incapable of including their effect explicitly. These models are based on the solution of the Navier-Stoke equations, which combine mass and momentum conservation. The following equation describes conservation of mass for an incompressible fluid:

$$\frac{\delta\rho}{\delta t} + \frac{\delta(\rho u_i)}{\delta x_i} = 0 \tag{1}$$

The conservation of momentum is described by the following transport equation:

$$\frac{\delta(\rho u_i)}{\delta t} + \frac{\delta(\rho u_j u_i)}{\delta x_j} = \frac{-\delta p}{\delta x_i} + \frac{\delta\tau_{ij}}{\delta x_j} + \delta \tag{2}$$

Eq. (2) includes the source term S to allow inclusion of the Coriolis Effect in the model and is defined as $(fv - fw - fu, fu)$, where the Coriolis coefficients are calculated as $f = 2\Omega sin(\phi)$and $f = 2\Omega cos(\phi)$, using the Earth's rotation speed.

The energy conservation is described by the following transport equation:

$$\frac{\delta(\rho E)}{\delta t} + \frac{\delta(u_i(\rho E + p))}{\delta x_i} = \frac{\delta}{\delta x_j}\left[\left(k + \frac{c_p * \mu_t}{Pr_t}\right)\frac{\delta T}{\delta x_j} + u_i(\tau_{ij})_{eff}\right] \tag{3}$$

For an incompressible fluid such as pure water at ordinary temperatures and pressures, density may be considered as constant. However, in the ocean density is a complicated function that depends upon the pressure, temperature and salinity. In practice, ocean density may be considered independently of pressure and linearly dependent on temperature and salinity. This yields the following equation of the state for the ocean:

$$\rho = \rho_0[1 - \alpha(T - T_0) + \beta(S - S_0)] \tag{4}$$

Fig. 2. Estero Elefantes. The red square shows a close up of the location of the cages. The yellow arrow shows the location of the ADCP (45°39′16.50″S–73°35′59.40″W). (For interpretation of the references to colour in this figure legend, the reader is referred to the web version of this article.)

where $\rho_0 = 1028$ (kg/m^3), $\alpha_0 = 1.7$ e-4 (K^{-1}), $\beta_0 = 7.6$e-4 (−), $T_0 = 283$ (K), $S_0 = 35$ (−).

To include salinity in Eq. (3) we used the following generic transport equation:

$$\frac{\delta\rho\phi}{\delta t} + \frac{\delta}{\delta x_i}\left(\rho u_i\phi - \Gamma\frac{\delta\phi}{\delta x_i}\right) = S_\phi \tag{5}$$

where ϕ is an arbitrary scalar, in this case salinity, Γ is the diffusion coefficient and S_ϕ is a source term.

2.1.1. Turbulence model: wall-modeled large Eddy simulation (WMLES)

Turbulent flows have high spatial and temporal variability. They are highly unstable, nonlinear and efficient at mixing themselves and the properties they transport (energy, salinity, chemical species, etc.) due to macroscopic fluctuations of fluid parcels. The simulation of large eddies (LES) is based on the observation that small-scale turbulent structures have a more universal behavior than the large-scale turbulence. This allows the contribution in terms of energy and momentum transport associated with the large turbulent structures to be calculated directly, while the small structures are modeled, thus originating the need of sub-grid models.

In the LES model, any flow variable U may be composed into a filtered part $\bar{U}$ (large scales) and a non-filtered thus modeled part, U' (small scales).

$$U = \acute{U} + U' \tag{6}$$

The space filtered variable is defined as:

$$\acute{U}(\vec{r_o}, t) = \int_D U(\vec{r}, t)G(\vec{r_o}\,|, \vec{r}, \Delta)d\vec{r} \tag{7}$$

where D is the complete domain of the flow, G is the filter function and $\vec{r}$ is the vector position. The filter function determines the structure and size of the small-scale turbulence. This function depends on the difference $(\vec{r_o} - \vec{r})$ and on the filter width $\Delta = (\Delta_1\Delta_2\Delta_3)^{\frac{1}{3}}$.

The filter function takes the following form:

$$G = \begin{cases} \frac{1}{\Delta^3}, \wedge\ si\ |r_o - r| \le \frac{\Delta}{2} \\ 0, \wedge\ otherwise \end{cases} \tag{8}$$

The derivation of the complete set of filtered Navier-Stokes equations is complex and beyond the focus of this study. After applying the filtration process, the momentum equation is summarized as:

$$\frac{\delta(\rho\acute{u}_i)}{\delta t} + \frac{\delta\rho(\acute{u}_i\acute{u}_j)}{\delta x_j} = \frac{-\delta\acute{p}}{\delta x_i} + \frac{\delta}{\delta_j}(\sigma_{ij}) - \frac{\delta\tau_{ij}}{\delta x_j} \tag{9}$$

where σ_{ij} is the tensor of forces associated with the molecular viscosity and $\tau_{ij}$is the tensor of sub-grid forces that results from filtering the Navier-Stokes equations and which must be modeled. Similar to RANS models, the LES model uses the Boussinesq's Hypothesis to calculate the sub-grid stresses

$$\tau_{ij} = -2\mu_T\acute{S_{ij}} \tag{10}$$

where $-S_{ij}$is the strain rate of the sub-grid scales and is defined as:

$$\acute{S_{ij}} = \frac{-1}{2}\left(\frac{\delta\acute{u}_i}{\delta x_j} + \frac{\delta\acute{u}_j}{\delta x_i}\right) \tag{11}$$

and μ_T is the sub-grid eddy viscosity which must be modeled.

In the Smagorinsky model, the sub-grid eddy viscosity is modeled as:

$$\mu_T = \rho L_s^2\ |\acute{S}| \tag{12}$$

where L_S is the length of the mixture and is expressed as:

$$L_S = min(kd, C_s\Delta) \tag{13}$$

k is the Von Kármán constant, d is the nearest wall distance, C_S is the Smagorinsky constant and Δ is the local grid scale, which is usually approximated as:

$$\Delta = V^{\frac{1}{3}} \tag{14}$$

where V is the cell volume.

To use a LES model to describe wall bounded turbulent flows, computational grids must be built with sufficiently fine resolution to capture the smallest structures generated within the boundary layers, which implies high computational cost and calculation time. The WMLES model, a variant of the LES model, allows describing flows surrounded by walls without needing very fine grids in the zones associated with the boundary layers. Sub-grid viscosity is modeled in the WMLES model as:

$$\mu_T = \rho \tag{15}$$

where d_w is the distance to the wall, S is the magnitude of the strain

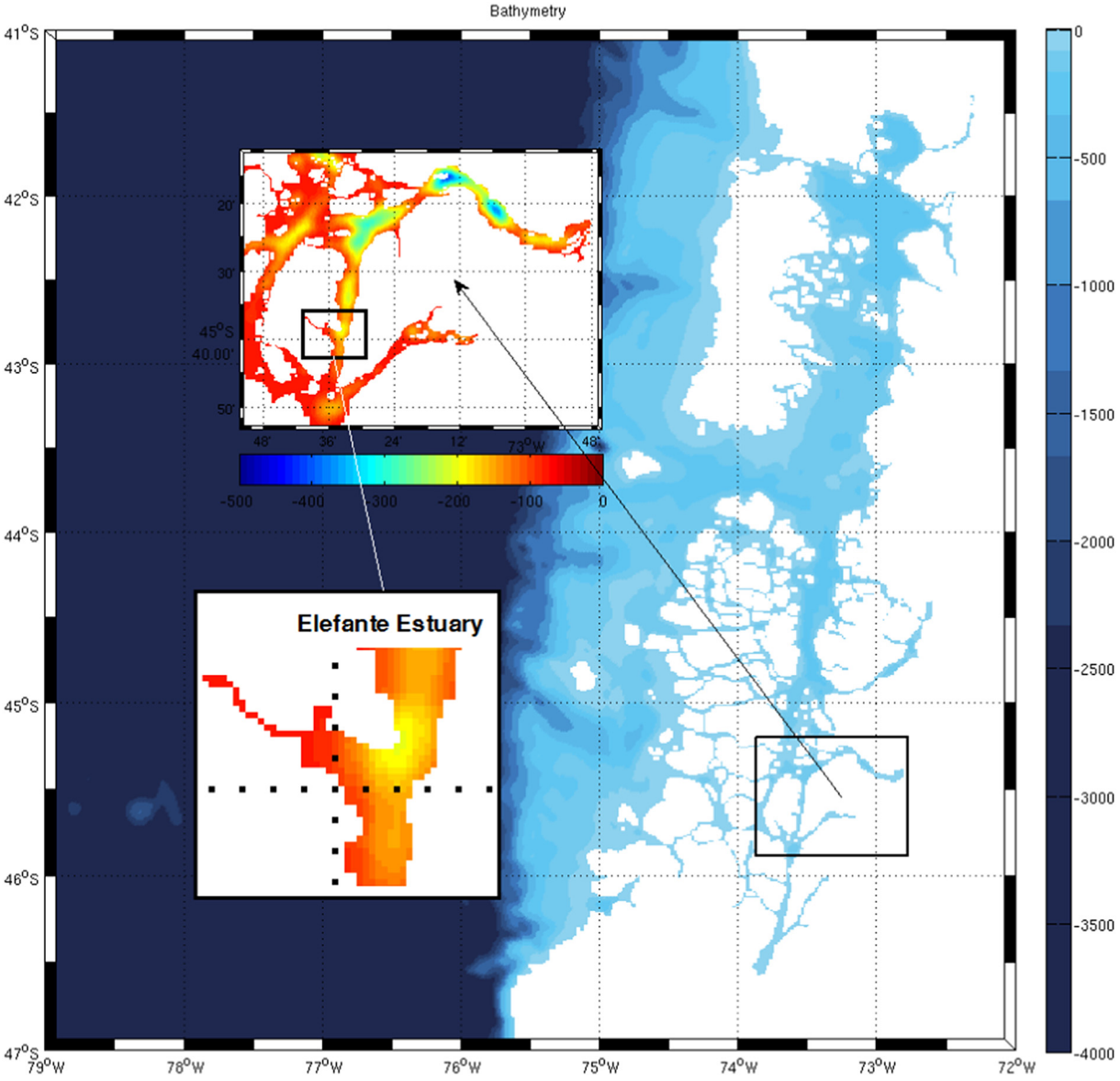

Fig. 3. Domain used in regional simulation using CROCO.

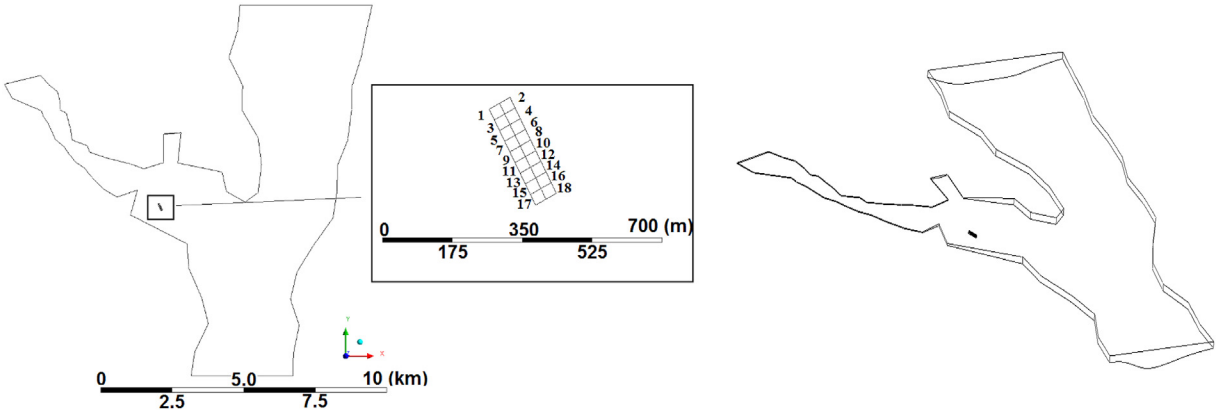

Fig. 4. Views of the 3-D geometric model.

rate, k = 0.41 and C_{Smag} = 0.2 are constants. Another advantage of WMLES over the conventional LES model lies in the way the local grid scale is calculated. In the conventional model, the local grid scale is calculated as in Eq. (14). However, this approximation is valid for isotropic or nearly isotropic grids, which implies to build computational grids that are too dense in number of cells and therefore result in

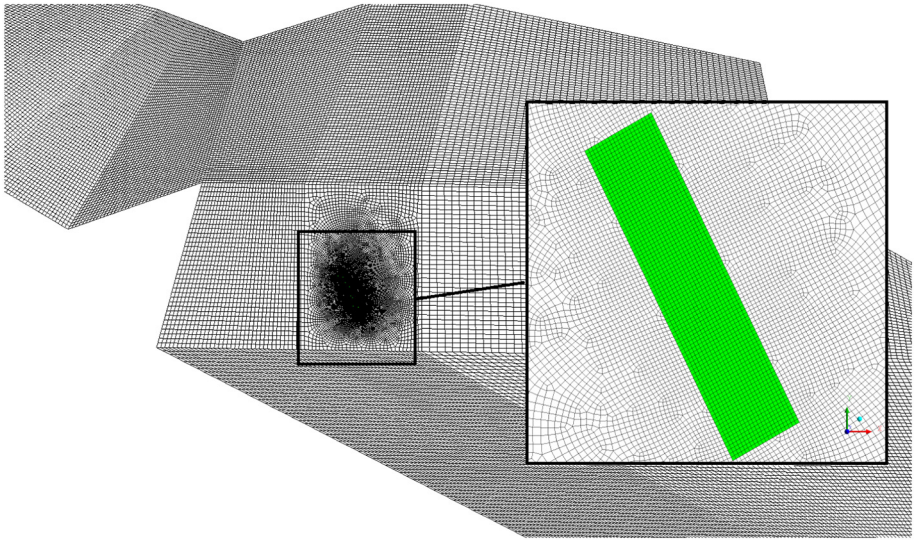

Fig. 5. Computational grid with the cages installed. Close up of the area where the cages are located.

Table 1
Porous jump boundary condition parameters.
From Cornejo et al., 2014.

Net	C_2 (m^{-1})	α (m^2)	Δ (mm)
Low drag	58.6	2.4e6	1.24
Medium drag	103.9	5.7e5	2.05
High drag	276.4	4.2e5	1.63

Table 2
Grid convergence analysis. Distribution of aspect ratios in computational grids.

	0–4	4–8	8–11	11–16	16–20
Coarse Grid	45.42%	30.96%	13.9%	6.09%	2.85%
Fine Grid	73.57%	19.31%	7.12%	–	–

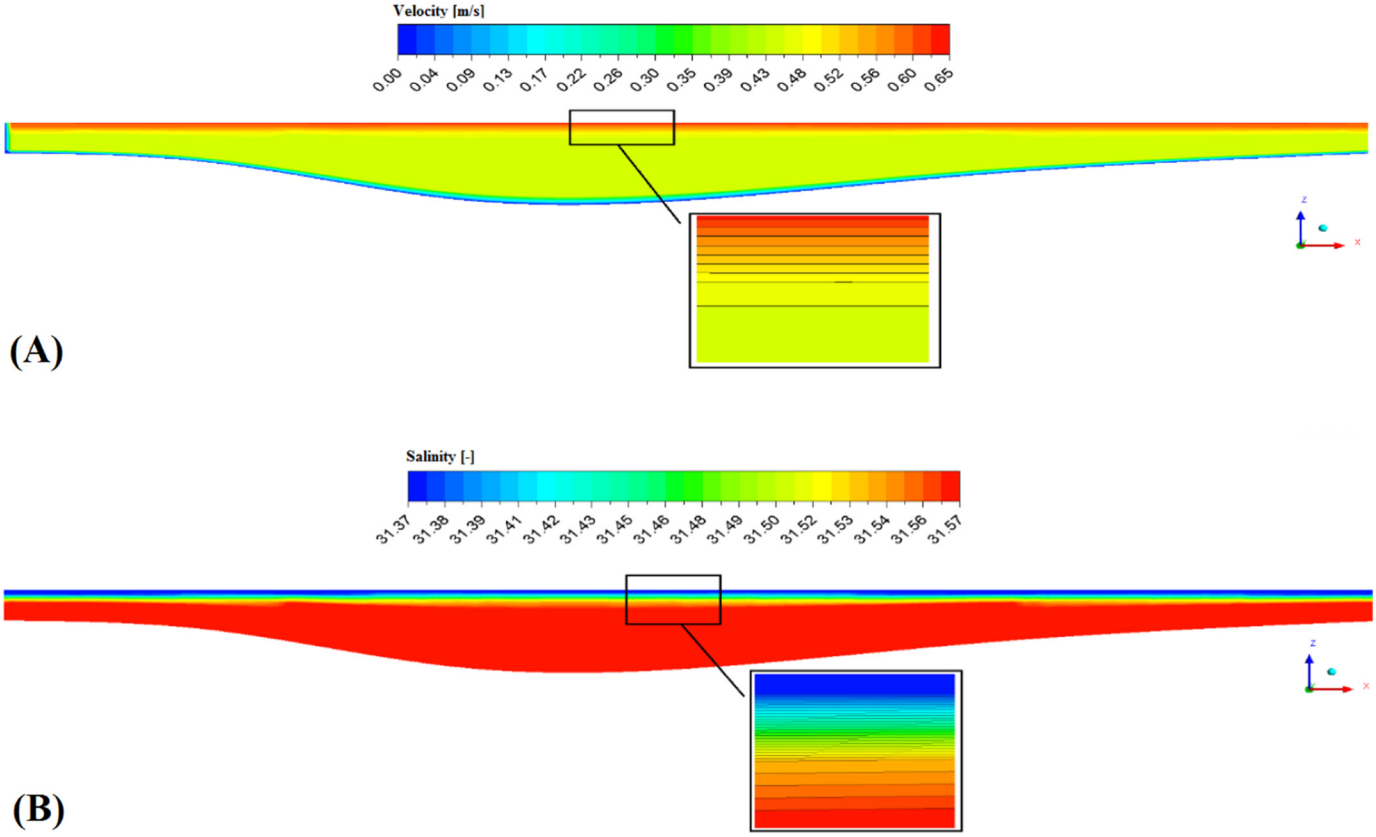

Fig. 6. Domain initialization. (A) Velocity magnitude and (B) Salinity at *velocity inlet* at $t = 0$ s.

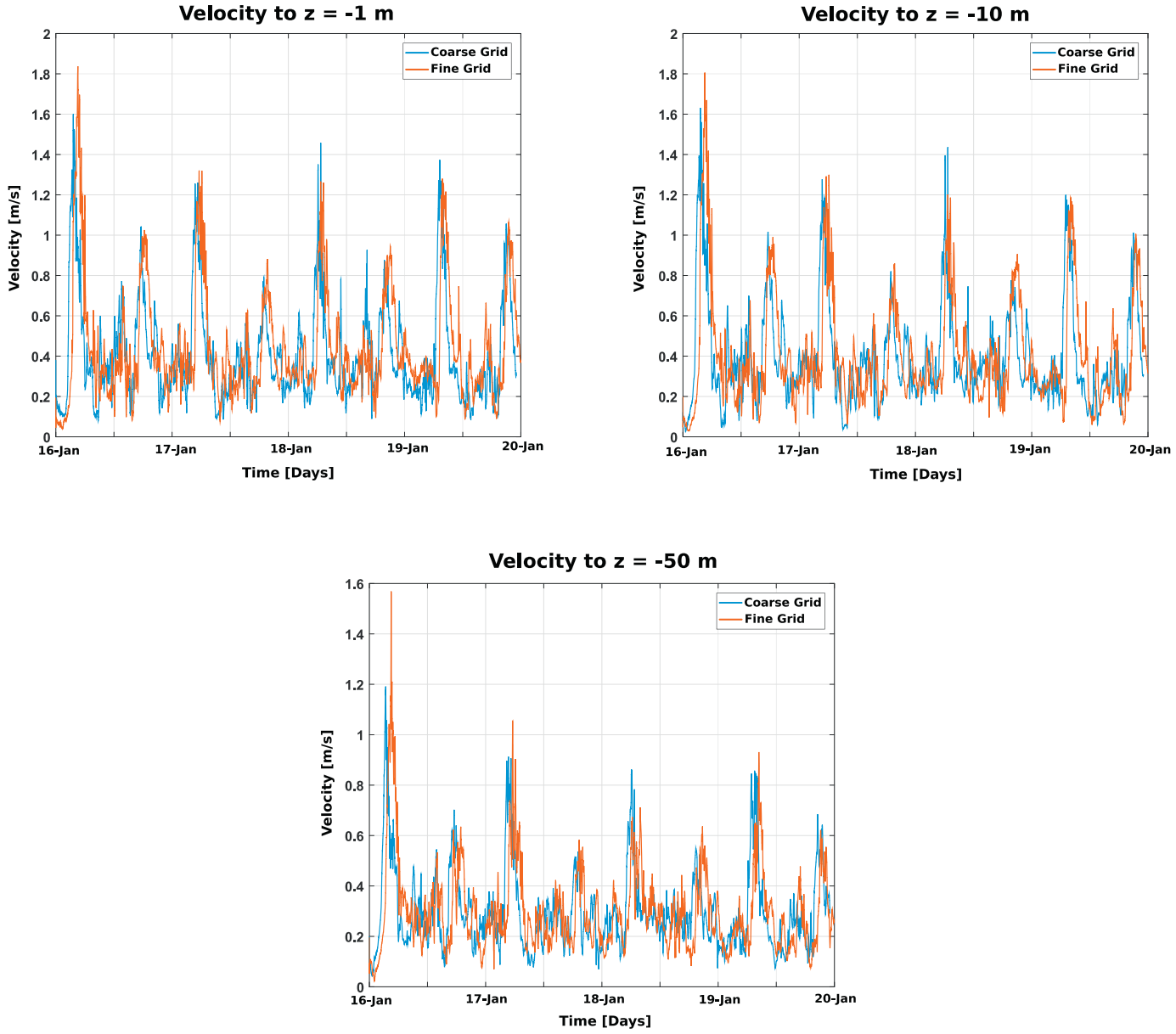

Fig. 7. Grid convergence analysis. Comparison of eulerian time series of velocity magnitude at different depths over a vertical line 1 km east of the cages.

simulations with high computational cost. The WMLES model allows higher anisotropy, as well as using a term that includes a function of wall damping. Thus the local grid scale is calculated as:

$$\Delta = min(max(C_w d_w; C_w h_{max}; h_{wn}); h_{max}) \quad (16)$$

where h_{max} is the maximum length of the cell edge, h_{wn} is the normal grid spacing and $C_w = 0.15$ is a constant.

2.1.2. Modeling the hydrodynamic effect of the cages

From the hydrodynamic point of view, salmon cages represent a momentum sink for the incident current. To describe the effects over the flow by the cage installation was used a porous jump boundary condition. The cage is considered as a thin permeable membrane in which the correlation between drag forces (pressure drop) and inlet velocity magnitude are known. This correlation is governed by Eq. (17), which is a combination of Darcy's Law and an additional inertial loss term.

$$\Delta P = -\left(\frac{\mu}{\alpha} v + C_2 \frac{1}{2} \rho v^2\right) \Delta m \quad (17)$$

where μ and ρ are respectively the viscosity and fluid density in which the cage is immersed, α is the permeability of the medium, C_2 is the coefficient of pressure loss, v is the normal velocity of the porous face and Δm is the thickness of the cage net. Both α and C_2 are properties of each net and must be estimated experimentally or from some correlation available in the literature. For this study we used the porosity parameters reported by (Cornejo et al., 2014).

3. Simulation

3.1. Methodology

Fig. 1 shows the flow diagram used in the proposed modeling methodology. Time and space-dependent data of velocity, temperature and salinity to satisfy the boundary conditions of the high-resolution LES model were obtained from a regional ocean simulation employing the CROCO model. To implement this dependence of the input data on the boundary conditions of the LES model it was necessary to use user-defined functions (UDF) in ANSYS FLUENT. Two additional UDF were

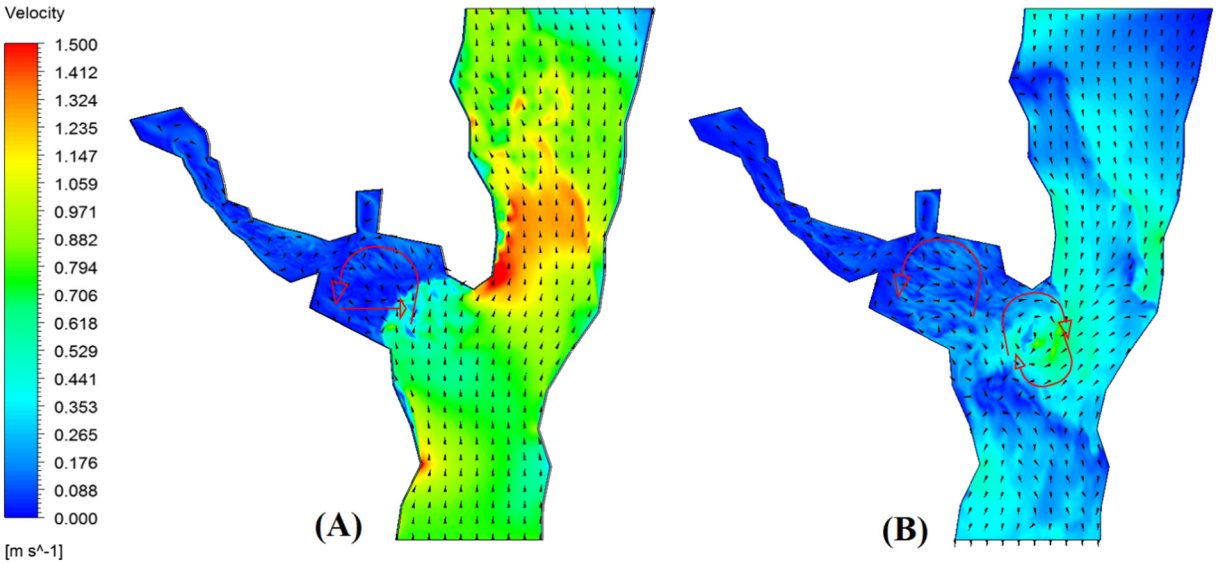

Fig. 8. Velocity field superimposed on contour of velocity magnitude on a plane at 10 m depth. (A) Northward current. (B) Southward current.

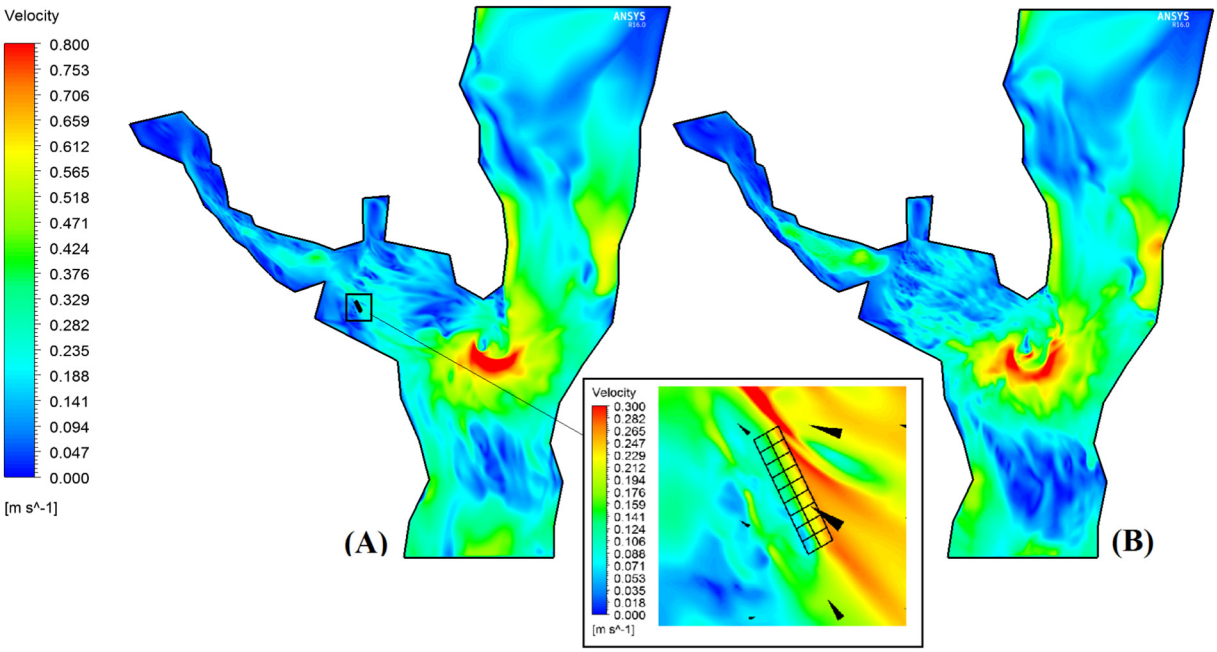

Fig. 9. Contours of velocity magnitude. (A) Simulation with cages. (B) Simulation without cages.

implemented to represent density as a linear dependent function of temperature and salinity and to initialize the model domain with a stratified water column. The results of the ANSYS FLUENT simulation were compared with the velocity components (u,v) obtained from an ADCP (u′,v′) located SE of the cages to verify the physical coherence of the model predictions.

3.2. Study case

The study area is located in the Moraleda Channel (44°57′S, 73°21′W), XI Region, Chile. This is an extensive channel from which several arms come off. The salmon cages are located specifically in one of the arms of the channel called the Estero Elefantes (46°30′S; Fig. 2). The study period for the regional-scale model was one moth and corresponds to January 2011. The high-resolution WMLES simulation included 4 days between January 16th and 20th, 2011.

3.3. Regional simulation

To provide the boundary conditions for the high-resolution WMLES simulation associated with the study case, we implemented a nested regional ocean simulation of the zone of interest using CROCO (Coastal and Regional Ocean COmmunity model). This model is a new version of the ROMS_AGRIF model (Debreu et al., 2012), which includes a non-hydrostatic solver in order to resolve very fine scales (especially in coastal zones) and their interaction with larger scales. It is a tri-dimensional, free-surface non-hydrostatic numerical model that solves the primitive equations over vertical coordinates or that follow the bathymetry (Shchepetkin and McWilliams, 2005) and an Arakawa-C-type (Arakawa and Lamb, 1981) structured grid using the finite volumes method. It uses two modes to solve the primitive equations, an external mode with shorter time intervals for barotropic processes and an internal mode with less restrictive time intervals for baroclinic processes. It can use different turbulence models to solve the vertical

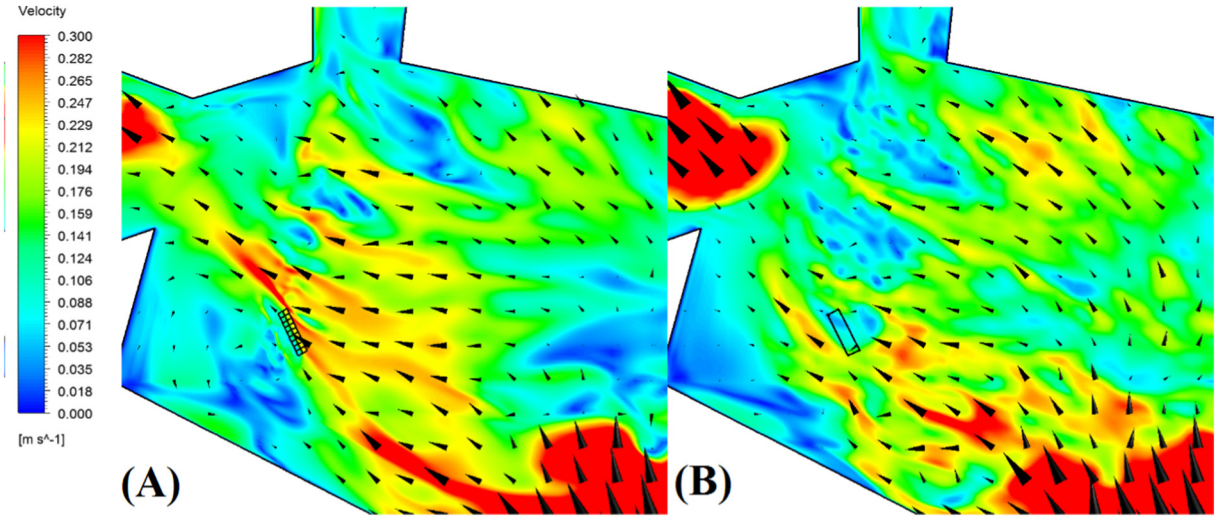

Fig. 10. Velocity field superimposed on contours of velocity magnitude. (A) Simulation with cages. (B) Simulation without cages. The black rectangle is the virtual location of the cages.

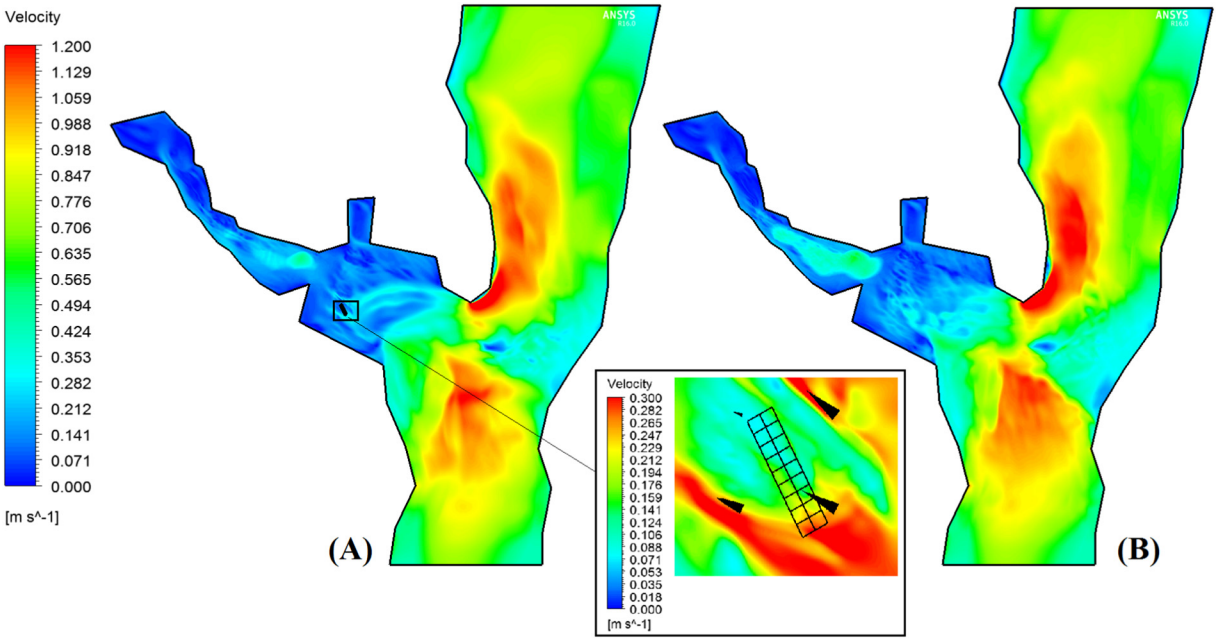

Fig. 11. Contours of velocity magnitude. (A) Simulation with cages. (B) Simulation without cages.

mixing. Horizontal mixing is solved with a Laplace operator and a diffusion coefficient that depends on the mean flow gradients.

We designed a nested system with two domains of different spatial resolution, ~1.2 km (parent domain) and ~400 m (nested domain), both with 32 vertical levels, using a model configuration similar to Olivares et al. (2015). Both domains used GEBC008 bathymetry (Sandwell et al., 2002) improved with data from nautical charts of the Hydrographic and Oceanographic Service of the Chilean Navy (SHOA). The coastline is edited to consider the main fjords and channels and to represent the circulation of the zone in the best possible way. The simulation period was January 2011. The lateral forcing and the initial condition were obtained from the ECCO product (Wunsch et al., 2009). The free surface was forced by winds and heat fluxes obtained from NCEP2 (Kanamitsu et al., 2002). The tide was added by calculating the tide coefficients obtained from the TPX07 database (Egbert and Erofeeva, 2002). For the purpose of this study we only used the outputs from the ~400 m resolution domain. Fig. 3 shows the calculation domain used in the simulation, as well as the bathymetry of the zone.

3.4. WMLES simulation

The channel geometry, the cage farm and the location of the ADCP are shown in Fig. 4. The coastline was simplified to build the computational grid considering that the resolution of the bathymetry employed is coarser than the resolution of the coastline. The farm consists of 18 cages positioned in tandem with dimensions of 30 × 30 × 30 m each. The reference axes were oriented with X+ to the East and Y+ to the North. For the grid convergence analysis we built a “coarse” grid with 850,000 hexahedral elements and a “fine” grid with approximately 2.1 million hexahedral elements. The number of elements in each grid was defined based on the aspect ratio which it was desired to achieve in the discretization cells. To use the LES model or its variants is important the degree of anisotropy of the computational grid. We limited the maximum aspect ratio to 11 and 20 for the fine and coarse grids, respectively. Table 2 shows the cells aspect ratios distribution of the computational grids.

To build the computational grid including the salmon cages we

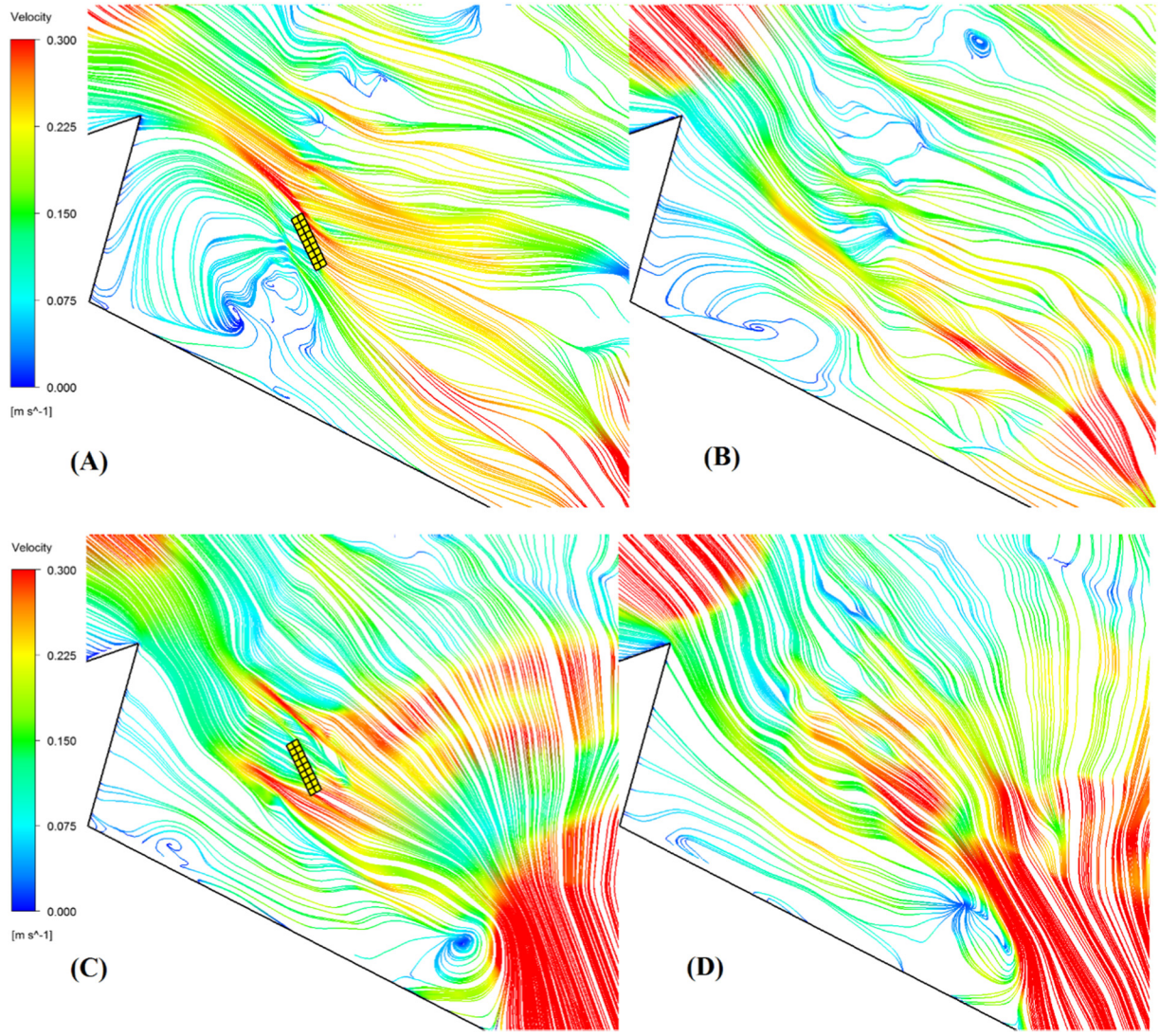

Fig. 12. Pathlines colored by velocity magnitude in a plane at 4 m depth. (A) Southward flow with cages. (B) Southward flow without cages. (C) Northward flow with cages. (D) Northward flow without cages.

modified the coarse grid. Approximately 1.45 million elements were used with a maximum aspect ratio equivalent to 20. The vertical resolution used near the surface was 3 m in all the grids considered. Fig. 5 shows the computational grid that included the cages with a close up of the zone where they are located. The boundary condition in open boundaries of the channel were taken from the regional model outputs; the walls that delimit the domain other than the upper surface were described as walls assuming the no-slip condition and the wind forcing in the X and Y directions were fixed on the surface of the channel by using NCEP2 (Kanamitsu et al., 2002) database and assumed constant in space in all the upper surface but variable in time. Cages were described using a porous jump condition with permeability values equal to the high drag condition given in Table 1.

Fig. 6 shows the contours of velocity and salinity generated in one of the open boundaries of the model domain for the initial condition $t = 0$ s.

4. Results

4.1. Grid convergence analysis

We performed two simulations without considering the salmon cages to analyze the sensitivity of the aspect ratio and the number of cells considered in the grid over the model predictions. Both computational grids were described in Table 2. The simulation period considered by simulations was January 16th–20th, 2011. Fig. 7 shows a eulerian measurement of velocity magnitude for both grids at different depths over a line drawn vertically from the channel surface to the bottom 1 km east of the cages. There is similarity in the temporal variability and in the peak velocity of the two grids. A comparison of velocity magnitude contours between the grids at 1 m depth at the beginning of the third day also predicts a similar distribution of velocity magnitude. Thus the simulations employing grids with different cells density and aspect ratio describe the flow field similarly.

4.2. Hydrodynamics of the Moraleda Channel adjacent to the Estero Elefantes

The tidal regime in the Moraleda Channel is semidiurnal (Fierro, 2001, 2008) and the current direction changes every 6 h. Fig. 8 shows a comparison of vector fields superimposed on a contour of velocity magnitude in a plane at 10 m depth. The current conditions were compared in the respective maximum velocities generated during an interval of 6 h for the last day simulated. When the current moves from S to N (Fig. 8A) a large eddy is generated in the cage zone that rotates counterclockwise. There is also a large water mass with high velocity

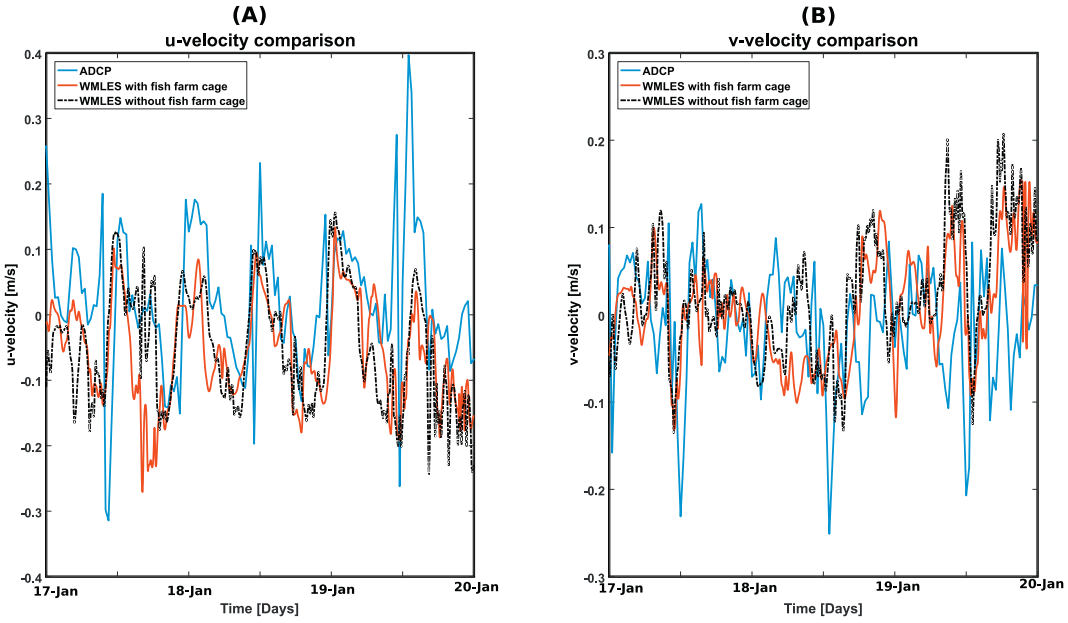

Fig. 13. Comparison between ADCP measurement and the computational model prediction for: (A) Velocity component u. (B) Velocity component v.

that generates a detachment near the coastline produced by the division of the main branch of the channel. In contrast, when the current moves from N to S (Fig. 8B) two eddies are generated which rotate in opposite directions; one clockwise eddy in the center of the channel possibly generated by detachment of the water mass near the coastline, and a second anticlockwise eddy located in the cage area induced by the rotation of the first eddy. Thus depending on the current direction two different circulation modes are generated in the channel with different locations of recirculation and/or retention zones and zones of high mixture, both characterized by a highly unstable shear flow composed of a large number of turbulent structures.

4.3. Hydrodynamics effect of cages in the Moraleda Channel

Figs. 9, 10, and 11 show comparisons of the distribution of velocity magnitudes in a general view and a close up in the zone near the cages for both cases, when the current flows from N to S and from S to N, respectively. When the current flows southwards the distribution and the magnitudes present in the velocity field are modified due to the installation of the cages. This difference is reflected both in the main area of the channel and where the cages are located. Fig. 10 shows a close up of the zone where the cages are located. Their installation modifies the velocity field in areas adjacent to them, generating areas of low velocity magnitude and therefore less intense mixing that are not present in the simulation performed without cages, which is approximately one order of magnitude weaker. There is also a “shadow zone” of low velocity magnitude behind the cages that generates a reduction in velocity magnitude of about 50% with respect to the incident velocity magnitude. The same occurs when the tide moves from S to N. There is also a general modification of the velocity field along the channel (Fig. 11), the velocity field near the cages was also modified, the areas of high and low velocity magnitude were displaced as a result of cages installation and a “shadow zone” of low velocity magnitude is formed behind the cages with a decrease in velocity magnitude similar to the previous situation. Fig. 12 shows a comparison of the pathlines for the current directions. When the current flows from N to S the pathlines that pass through the cages have their trajectory modified. This generates a recirculation and/or retention zone right behind the cages that includes all the area near the coastline. The size of the area where recirculation is generated is much greater than the natural recirculation generated when the cages are not present. When the current flows from S to N the path lines are modified above the location of the cages, forming an eddy with the size of the salmon farm that is not generated when the cages are not present. These results show that the salmon cages not only modify the direction and magnitude of the local velocity field generating a new recirculation and/or retention zones and changing the circulation locally, but they also affect circulation far from them due to the propagation of the perturbations they generate in the natural hydrodynamics of the channel.

4.4. Comparison with field measurements

To verify the physical coherence of the model predictions we contrasted velocity data obtained in the zone by an ADCP located SE of the cages with the results predicted by simulations with and without considering the installation of cages for the period of time between January 17th and 20th, 2011. Fig. 13 shows a comparative plot for the time series of the velocity components in the ADCP location at a depth of 4 m. The model results including the cages installation predicts well the instantaneous variations in velocity magnitude picks and in general the tendency of the temporal velocity magnitude variations. Fig. 14 shows four quantile plots comparing the distribution between velocity components measured by ADCP and the predicted velocity components obtained from the model with and without cages. The distribution of the u velocity component from -0.15 m/s to 0.15 m/s was similar in the ADCP data and model predictions. However, the v velocity component in the model with cages had a greater range of velocities with a distribution similar to the experimental measurements compared to the results without cages. For all cases, the red area in the graphs indicates the values for which the distribution predicted by the model is similar to the distribution of the field measurements.

4.5. Potential transport of organic and inorganic materials released during the production process

We analyzed the transport of material discharged inside the cages by the implementation of a multiphase flow in which the phases were the water volume initially enclosed by the cages and the remaining water volume in the channel. Fig. 15 shows the volume fraction of water volume initially enclosed in the cages in the whole channel every 6 h. The water transport was highly influenced by the direction of the current spreading out in the channel. At the end of the day a large part

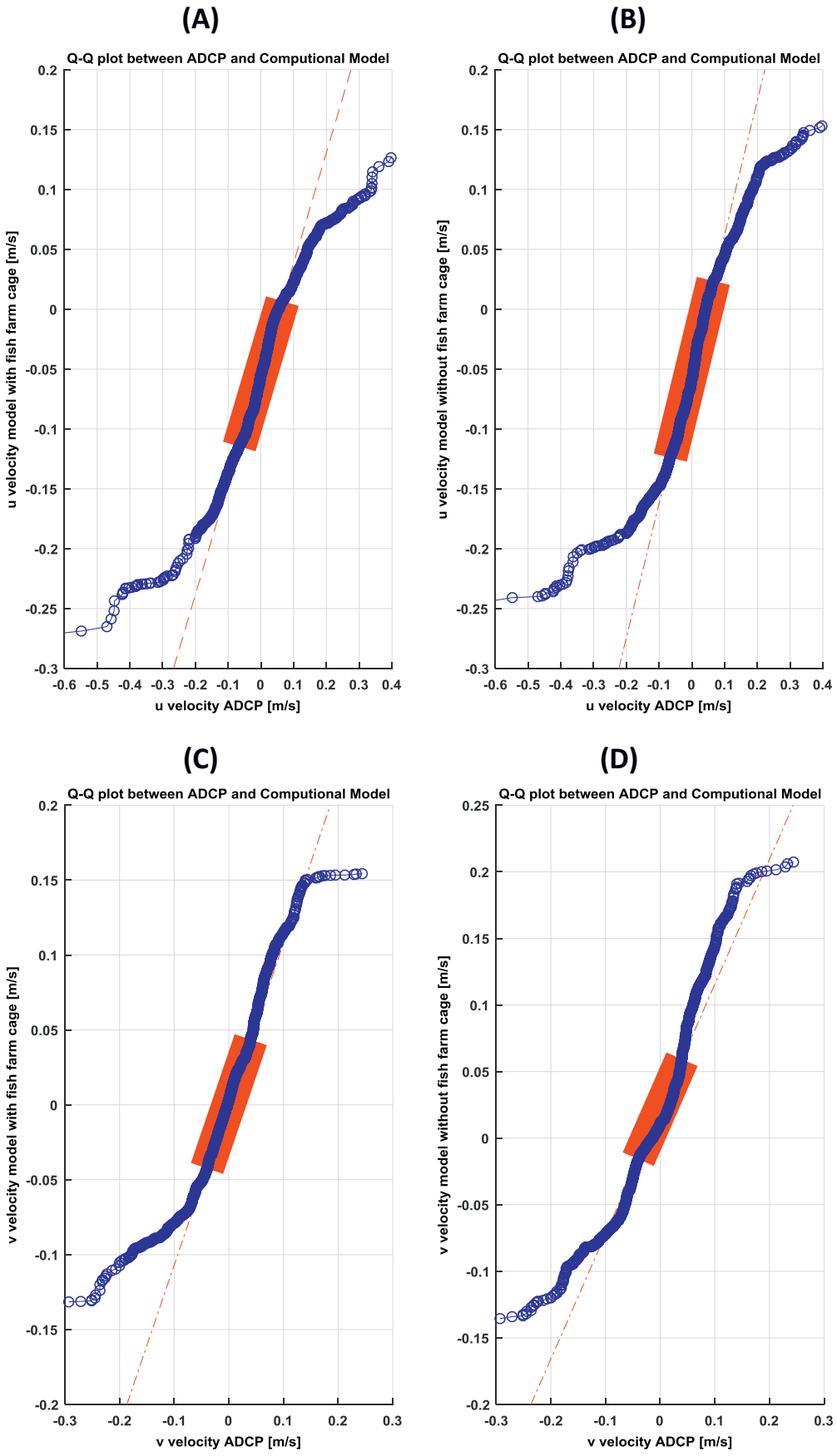

Fig. 14. Q-Q plot of the velocity components (u, v) between the ADCP measurements and computational model predictions with cages (A–C) and without cages (B–D).

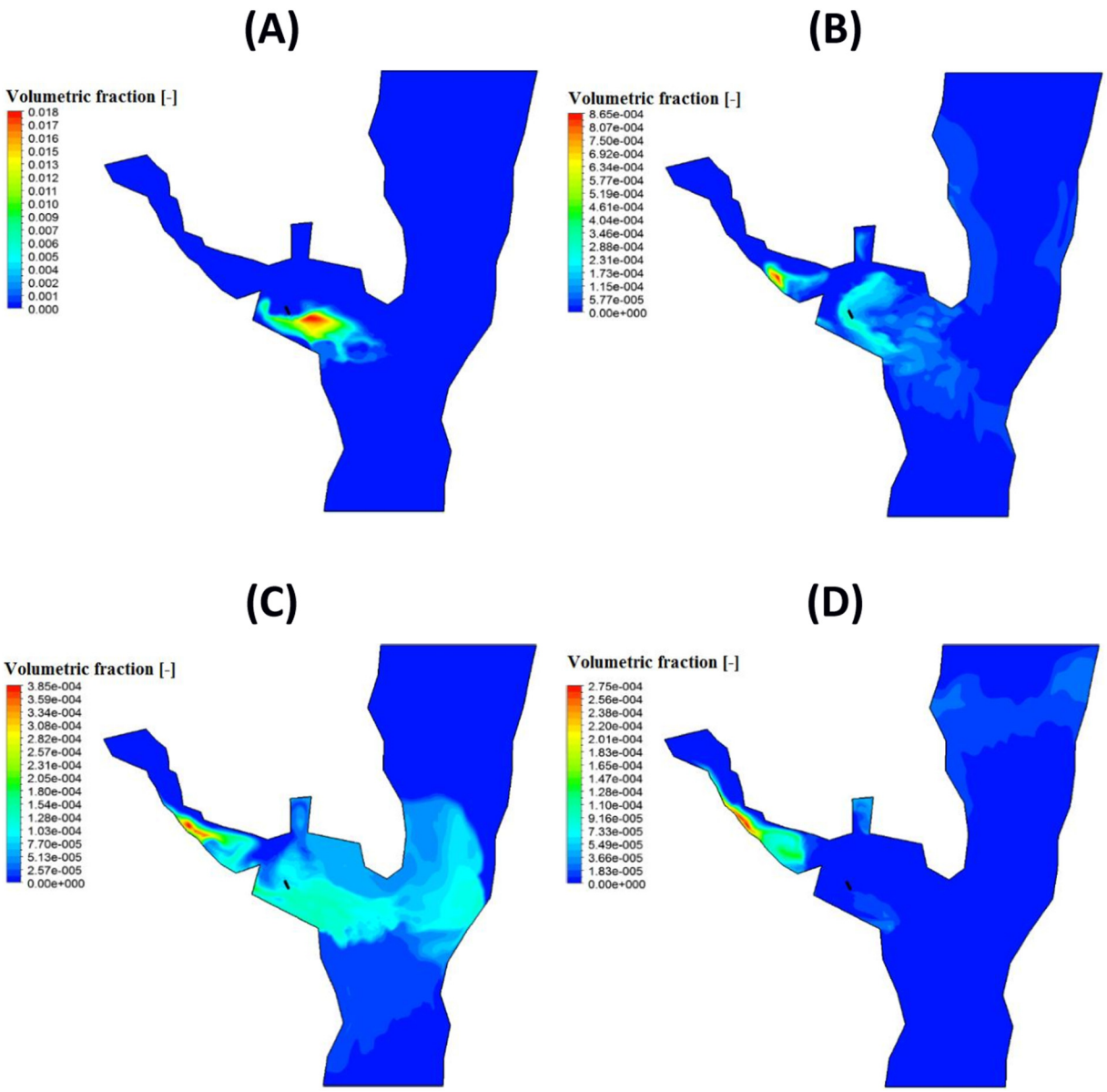

Fig. 15. Transport of water initially enclosed by cages. Contour of volume fraction of water initially enclosed by cages in a plane at 4 m depth every 6 h during the last day of simulation (A) Hour 6. (B) Hour 12. (C) Hour 18. (D) Hour 24.

of the water volume originally enclosed in the cages left the channel. However, a certain amount remained stagnant in the left side of the channel, spreading out as the day advanced. Fig. 16 shows the evolution of the volume fraction of water initially enclosed by cages transported by currents within cages 1 and 17 at different depths. The results indicate that after 1 h the water that was initially enclosed left the cages completely. However, due the large eddies that are generated in this zone it returns to the cages 6 h later, although at much lower concentration, and slowly decreases during the day. This behavior was the same at both depths.

5. Discussion

To assess the effect due to the installation of salmon cages on the local hydrodynamics of a channel or fjord it is important to understand the local circulation both around and within the cages. This may be done by field measurements, however, this is usually associated with long measurement times, high cost and long times of data processing (Langis, 2015). Numerical simulations appear as a good alternative or complementary tool to describe the local hydrodynamics of a specific geographic area. However, current regional ocean models cannot include the effect of fish farms in their simulation or describe the microscale fluid dynamic processes such as those associated with salmon cages, mainly due to the restriction of the maximum horizontal resolution of their computational grid elements. CFD models appear as an adequate alternative to describe geophysical fluid dynamics microscale processes in these kind of problems, however, they need to be forcing with realistic boundary conditions. Due to these limitations this study examined the coupling between a regional oceanographic model with non-hydrostatic solver and a high-resolution LES model including the salmon cages explicitly, with which we could analyze the hydrodynamic effects associated with the installation of farm cages under realistic conditions. This kind of coupling between mesoscale and microscale models is not new, it has been used, for instance, in atmospheric studies considering the interaction between mesoscale atmospheric models and CFD simulations (e.g. Li et al., 2010; Yamada and Koike, 2011).

To incorporate the hydrodynamic effects of cages it was necessary to

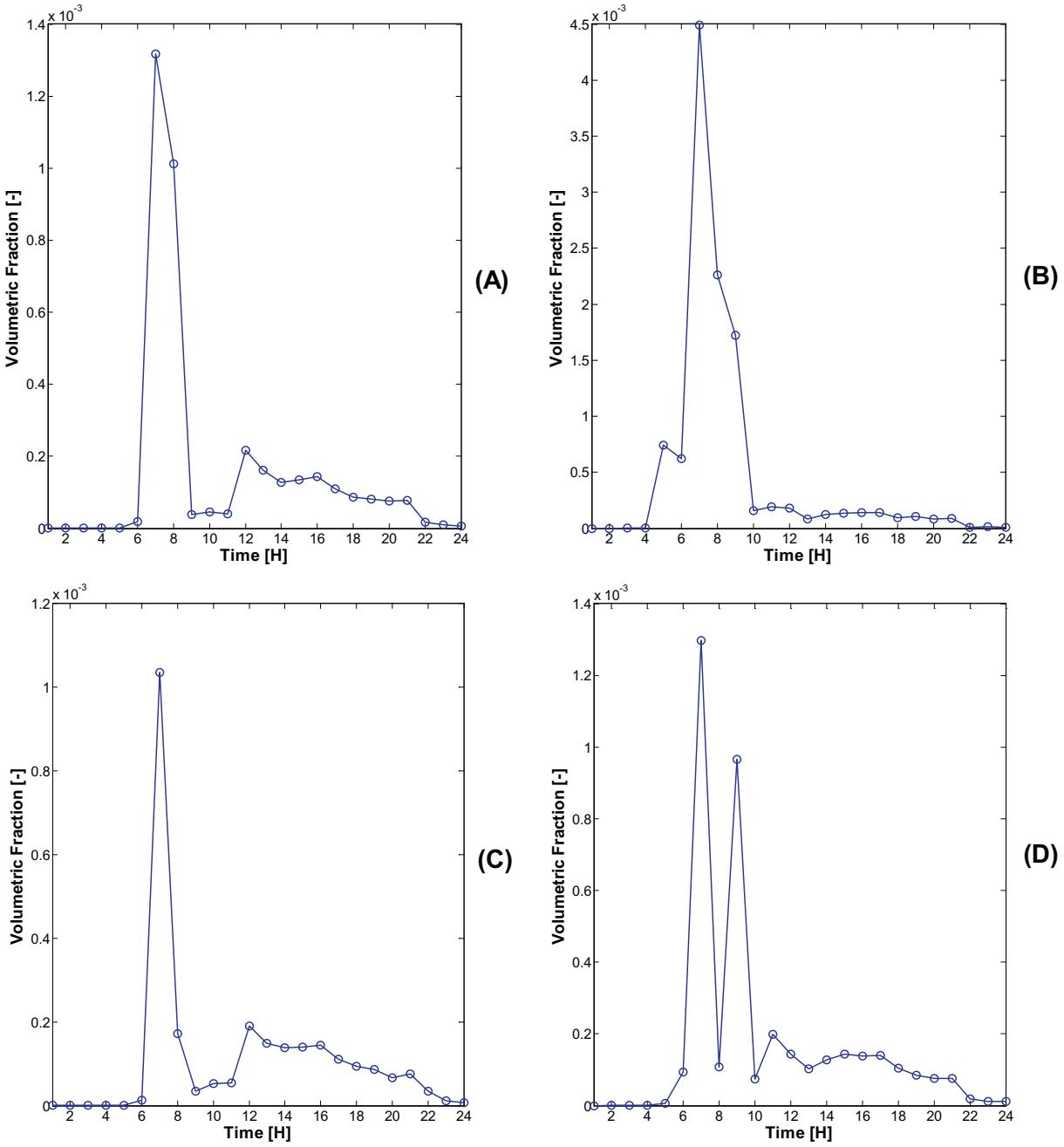

Fig. 16. Evolution of the volume fraction of water initially enclosed by cages at two points located within cages 1and 17 at different depths. (A) Cage 1 at 5 m. (B) Cage 17 at 5 m. (C) Cage 1 at 15 m. (D) Cage 17 at 15 m.

describe them explicitly with a porous jump boundary condition. This condition assumes that the relation between pressure drop and velocity magnitude of the incident current is known a priori. Thus the porosity parameters must be calibrated correctly by experimental measurements (Tsukrov et al., 2011). There are a number of factors to be considered to implement a model to describe the processes associated with the hydrodynamics of a fish farm in a realistic environment such as coastline, bathymetry, wind forcing, currents, stratification of the water column, etc. However, the definition of the control volume is even more important. It is tempting to isolate a fish farm defining a regular local control volume with inlets, outlets and impermeable walls to study the hydrodynamics in the neighborhood of a fish farm as proposed in the study of Winthereig-Rasmussen et al. (2016). However, based on our results the circulation in a fjord or channel with broken coastline dominated by tides with temporal variability generates a highly unstable flow field influenced by the interaction of turbulent structures of various sizes that act and interact with the fish farm, generating a highly turbulent flow field in their neighborhood. Thus it is not possible to define a priori a regular local control volume imposing impermeable walls, inlets and outlets in the natural circumstances explained above. Instead it is recommendable to define the boundary conditions sufficiently far away from the salmon cages as was done in this study.

The results on the natural hydrodynamics of the channel showed the presence of large turbulent structures which constantly modify the magnitude and direction of the velocity field in the area near the cages. Thus the current impacts the salmon cages differently depending on the time of the day, generating different intensities of diffusion and mixing.

Comparison of the simulation results to field measurements showed that our model was capable of predicting the temporal variability of the velocity components, including abrupt changes in magnitude. However,

it had difficulty reproducing the magnitude of the velocity magnitude picks for certain times of the day. This is attributable to the limitations of the computational model in the resolution of the coastline and bathymetry and the use of constant wind shear on the channel surface, as well as the fact that the data taken for the boundary conditions from the regional ocean model results have an additional associated error.

The transport of wastes from the fish cages is an important environmental issue of salmon aquaculture due to the potential degradation of benthic habitats, eutrophication and risk of algal blooms (e.g. Findlay and Watling, 1997; Buschmann et al., 2009; Wang et al., 2012; Price et al., 2015). Hydrodynamics can also be crucial in influencing the incidence of diseases in salmon farms (e.g. Gustafson et al., 2007; Aldrin et al., 2010; Salama and Murray, 2011; Samsing et al., 2015). Thus, the interaction between the salmon cages and local hydrodynamic conditions must be considered in the spatial distribution of farms in the channels and fjords ecosystems (Cornejo et al., 2014). The proposed modeling approach is able to describe how a volume of water originally enclosed in the cages is transported in a given time, which is relevant, for instance, to the design of farming centers, to epidemiological studies and to estimate environmental impact, as a higher exchange could be beneficial for the fish inside the cages, but detrimental to the environment in terms of waste dispersal and disease propagation. This information should prove useful both for producers and the aquaculture management authority to consider solutions such as integrated management of aquaculture (e.g. Chopin et al., 2001; Neori et al., 2004).

6. Conclusion

We propose a modeling methodology to assess the hydrodynamic effects of a salmon farm in a channel or fjord based on a coupling between a regional oceanographic model and a high resolution LES model which explicitly included a fish farm. This method avoids the a priori definition of a regular local control volume with inlets, outlets and walls to study the hydrodynamics associated with salmon cages, which our results show would not be possible due to the highly turbulent flow within the channel. The proposed method is able to describe the effect of the fish cages on the local hydrodynamics of a particular geographic area in a realistic environment.

The circulation of the channel is dominated by a highly unstable flow produced by the temporal variation of the tide, associated with the coastline and the shear flow in the nucleus of the channel. The circulation mode is dependent on the current direction, forming turbulent structures that act and interact with the cages producing different effects on local hydrodynamics. The presence of the cages affects the velocity field in direction and magnitude,. both near the cages and in areas far from them. The reduction in velocity found behind the cages reached 50% of the incident current.

The model is able to predict the temporal variability of the current velocity components observed in ADCP data. However, the magnitude of some velocity peaks found in certain time of the day show differences between the model and field measurements attributable to the following limitations of the computational model: low resolution of the coastline and the bathymetry, constant wind forcing in space on the channel surface and possible errors in the results of the regional ocean model.

We found that a considerable part of the enclosed volume within the cages remains recirculating in a section of the channel during the rest of the day. The proposed modeling approach is a promising tool to study problems such as water reposition time within the cages, transport of organic and inorganic materials released from farm processes, and pathogens prevalence and dispersal.

Acknowledgements

This research was funded by the Interdisciplinary Center for Aquaculture Research (INCAR; FONDAP Project N°15110027; CONICYT). The model simulations were run at the Laboratory of Computational Mechanics of the Department of Mechanical Engineering of the University of Concepción (Concepción, Chile). ADCP and CTD measurements were obtained by Daniel Brieva and Juan Rodriguez in field work funded by Salmones Friosur S. A. Osvaldo Artal was funded by national CONICYT grant (CONICYT doctorate scholarship 21140379). Comments by two anonymous reviewers were greatly appreciated.

Appendix A. Supplementary data

Supplementary data to this article can be found online at https://doi.org/10.1016/j.aquaculture.2018.05.003.

References

Aldrin, M., Storvik, B., Frigessi, A., Viljugrein, H., Jansen, P.A., 2010. A stochastic model for the assessment of the transmission pathways of heart and skeleton muscle inflammation, pancreas disease and infectious salmon anaemia in marine fish farms in Norway. Prev. Vet. Med. 93, 51–61.

Arakawa, A., Lamb, V.R., 1981. A potential enstrophy and energy conserving scheme for the shallow water equations. Mon. Weather Rev. http://dx.doi.org/10.1175/1520-0493(1981)109<0018:APEAEC>2.0.CO;2.

Banco Central, 2017. Indicadores de Comercio Exterior, Cuarto trimestre 2016. Santiago, Chile. (50 pp.).

Bessonneau, J.S., Marichal, D., 1998. Study of the dynamics of submerged supple nets (applications to trawls). Ocean Eng. 25, 563–583. http://dx.doi.org/10.1016/S0029-8018(97)00035-8.

Bi, C.-W., Zhao, Y.-P., Dong, G.-H., Zheng, Y.-N., Gui, F.-K., 2014. A numerical analysis on the hydrodynamic characteristics of net cages using coupled fluid–structure interaction model. Aquac. Eng. 59, 1–12. http://dx.doi.org/10.1016/j.aquaeng.2014.01.002.

Bi, C.-W., Zhao, Y.-P., Dong, G.-H., Cui, Y., Gui, F.-K., 2015. Experimental and numerical investigation on the damping effect of net cages in waves. J. Fluids Struct. 55, 122–138. http://dx.doi.org/10.1016/j.jfluidstructs.2015.02.010.

Buschmann, A.H., Cabello, F., Young, K., Carvajal, J., Varela, D.A., Henríquez, L., 2009. Salmon aquaculture and coastal ecosystem health in Chile: analysis of regulations, environmental impacts and bioremediation systems. Ocean Coast. Manag. 52, 243–249. http://dx.doi.org/10.1016/j.ocecoaman.2009.03.002.

Buschmann, A.H., Tomova, A., López, A., Maldonado, M.A., Henríquez, L.A., Ivanova, L., Moy, F., Godfrey, H.P., Cabello, F.C., 2012. Salmon aquaculture and antimicrobial resistance in the marine environment. PLoS One 7 (8), e42724. http://dx.doi.org/10.1371/journal.pone.0042724.

Chamberlain, J., Stucchi, D., 2007. Simulating the effects of parameter uncertainty on waste model predictions of marine finfish aquaculture. Aquaculture 272, 296–311. http://dx.doi.org/10.1016/j.aquaculture.2007.08.051.

Chen, C., Liu, H., Beardsley, R.C., Chen, C., Liu, H., Beardsley, R.C., 2003. An unstructured grid, finite-volume, three-dimensional, primitive equations ocean model: application to coastal ocean and estuaries. J. Atmos. Ocean. Technol. 20, 159–186. http://dx.doi.org/10.1175/1520-0426(2003)020<0159:AUGFVT>2.0.CO;2.

Chen, W.B., Liu, W.C., Hsu, M.H., 2013. Modeling evaluation of tidal stream energy and the impacts of energy extraction on hydrodynamics in the Taiwan strait. Energies 6, 2191–2203. http://dx.doi.org/10.3390/en6042191.

Chopin, T., Buschmann, A.H., Halling, C., Troell, M., Kautsky, N., Neori, A., Kraemer, G.P., Zertuche-González, J.A., Yarish, C., Neefus, C., 2001. Integrating seaweeds into marine aquaculture systems: a key toward sustainability. J. Phycol. 37 (6), 975–986.

Cornejo, P., Sepúlveda, H.H., Gutiérrez, M.H., Olivares, G., 2014. Numerical studies on the hydrodynamic effects of a salmon farm in an idealized environment. Aquaculture 430, 195–206. http://dx.doi.org/10.1016/j.aquaculture.2014.04.015.

Debreu, Laurent, Marchesiello, Patrick, Penven, Pierrick, Cambon, Gildas, 2012. Two-way nesting in split-explicit ocean models: Algorithms, implementation and validation. Ocean Modelling 49-50, 1–21.

Doglioli, A., Magaldi, M., Vezzulli, L., Tucci, S., 2004. Development of a numerical model to study the dispersion of wastes coming from a marine fish farm in the Ligurian Sea (Western Mediterranean). Aquaculture 231, 215–235. http://dx.doi.org/10.1016/j.aquaculture.2003.09.030.

Egbert, G.D., Erofeeva, S.Y., 2002. Efficient inverse modeling of barotropic ocean tides. J. Atmos. Ocean. Technol. 19, 183–204. http://dx.doi.org/10.1175/1520-0426(2002)019<0183:EIMOBO>2.0.CO;2.

FAO, 2016. The State of World Fisheries and Aquaculture 2016. Contributing to Food Security and Nutrition for all. Food and Agriculture Organization of the United Nations, Rome (200 pp.).

Fierro, J., 2001. Tides in the Chilean coast. Hydro Int. 5 (1), 7–9.

Fierro, J.J., 2008. Tides in the austral Chilean channels and fjords. Pages 63–66. In: Silva, N., Palma, S. (Eds.), Avances en el conocimiento oceanográfico de las aguas interiores chilenas, Puerto Montt a Cabo de Hornos. Comité Oceanográfico Nacional - Pontificia Universidad Católica de Valparaíso, Valparaíso (162 pp.).

Findlay, R.H., Watling, L., 1997. Prediction of benthic impact for salmon net-pens based on the balance of benthic oxygen supply and demand. Mar. Ecol. Prog. Ser. 155,

147–157.
Fisheries and Oceans Canada, 2003. A scientific review of the potential environmental effects of aquaculture in aquatic ecosystems. Volume 1. Far-field environmental effects of marine finfish aquaculture (B.T. Hargrave); Ecosystem level effects of marine bivalve aquaculture (P. Cranford, M. Dowd, J. Grant, B. Hargrave and S. McGladdery); Chemical use in marine finfish aquaculture in Canada: a review of current practices and possible environmental effects (L.E. Burridge). Can. Tech. Rep. Fish. Aquat. Sci. 2450 (ix + 131 pp.).
Føre, M., Alver, M., Alfredsen, J.A., Marafioti, G., Senneset, G., Birkevold, J., Willumsen, F.V., Lange, G., Espmark, Å., Terjesen, B.F., 2016. Modelling growth performance and feeding behaviour of Atlantic salmon (*Salmo salar* L.) in commercial-size aquaculture net pens: model details and validation through full-scale experiments. Aquaculture 464, 268–278. http://dx.doi.org/10.1016/j.aquaculture.2016.06.045.
Fredriksson, D.W., DeCew, J., Swift, M.R., Tsukrov, I., Chambers, M.D., Celikkol, B., 2004. The design and analysis of a four-cage grid mooring for open ocean aquaculture. Aquac. Eng. 32, 77–94. http://dx.doi.org/10.1016/j.aquaeng.2004.05.001.
Fredriksson, D.W., DeCew, J.C., Tsukrov, I., Swift, M.R., Irish, J.D., 2007. Development of large fish farm numerical modeling techniques with in situ mooring tension comparisons. Aquac. Eng. 36, 137–148. http://dx.doi.org/10.1016/j.aquaeng.2006.10.001.
Gillibrand, P.A., Turrell, W.R., 1997. The use of simple models in the regulation of the inpact of fish farms on water quality in Scottish sea lochs. Aquaculture 159, 33–46.
Gustafson, L.L., Ellis, S.K., Beattie, M.J., Chang, B.D., Dickie, D.A., Robinson, T.L., Marenghi, F.P., Moffett, P.J., Page, F.H., 2007. Hydrographics and the timing of infectious salmon anemia outbreaks among Atlantic salmon (*Salmo salar* L.) farms in the Quoddy region of Maine, USA and New Brunswick, Canada. Prev. Vet. Med. 78, 35–56.
Hasegawa, D., Sheng, J., Greenberg, D.A., Thompson, K.R., 2011. Far-field effects of tidal energy extraction in the Minas Passage on tidal circulation in the Bay of Fundy and Gulf of Maine using a nested-grid coastal circulation model. Ocean Dyn. 61, 1845–1868. http://dx.doi.org/10.1007/s10236-011-0481-9.
Johansson, D., Juell, J., Oppedal, F., Stiansen, J., Ruohonen, K., 2007. The influence of the pycnocline and cage resistance on current flow, oxygen flux and swimming behavior of Atlantic salmon (*Salmo salar* L.) in production cages. Aquaculture 265 (1–4), 271–287.
Kanamitsu, M., Ebisuzaki, W., Woollen, J., Yang, S.K., Hnilo, J.J., Fiorino, M., Potter, G.L., 2002. NCEP-DOE AMIP-II reanalysis (R-2). Bull. Am. Meteorol. Soc. 83, 1631–1643. http://dx.doi.org/10.1175/BAMS-83-11-1631.
Langis, D., 2015. Arduino Based Oceanographic Instruments: An Implementation Strategy for Low-cost Sensors. California State Maritime Academy (47 pp.).
Larson, K.M., Löfgren, J.S., Haas, R., 2013. Coastal sea level measurements using a single geodetic GPS receiver. Adv. Sp. Res. 51, 1301–1310. http://dx.doi.org/10.1016/j.asr.2012.04.017.
Lee, C.W., Kim, Y.B., Lee, G.H., Choe, M.Y., Lee, M.K., Koo, K.Y., 2008. Dynamic simulation of a fish cage system subjected to currents and waves. Ocean Eng. 35, 1521–1532. http://dx.doi.org/10.1016/j.oceaneng.2008.06.009.
Li, L., Zhang, L., Zhang, N., Hu, F., Jiang, Y., Xuan, C.-Y., Jiang, W.-M., 2010. Study on the micro-scale simulation of wind field over complex terrain by RAMS / FLUENT modeling system. In: Fifth Int. Symp. Comput. Wind Eng. vol. 2. pp. 411–418. http://dx.doi.org/10.3724/SP.J.1226.2010.00411.
Löfgren, J.S., Haas, R., Johansson, J.M., 2011. Monitoring coastal sea level using reflected GNSS signals. Adv. Sp. Res. 47, 213–220. http://dx.doi.org/10.1016/j.asr.2010.08.015.
Neori, A., Chopin, T., Troell, M., Buschmann, A.H., Kraemer, G.P., Halling, C., Shpigel, M., Yarish, C., 2004. Integrated aquaculture: rationale, evolution and state of the art emphasizing seaweed biofiltration in modern mariculture. Aquaculture 231 (1–4), 361–391.
Olivares, G., Sepulveda, H.H., Yannicelli, B., 2015. Definition of sanitary boundaries to prevent ISAv spread between salmon farms in Southern Chile based on numerical simulations of currents. Estuar. Coast. Shelf Sci. 158, 31–39.
Panchang, V., Cheng, G., Newell, C., 1997. Modeling hydrodynamics and aquaculture waste transport in coastal maine. Estuaries 20, 14. http://dx.doi.org/10.2307/1352717.
Patursson, Ø., Swift, M.R., Tsukrov, I., Simonsen, K., Baldwin, K., Fredriksson, D.W., Celikkol, B., 2010. Development of a porous media model with application to flow through and around a net panel. Ocean Eng. 37, 314–324. http://dx.doi.org/10.1016/j.oceaneng.2009.10.001.
Price, C., Black, K.D., Hargrave, B.T., Morris Jr., J.A., 2015. Marine cage culture and the environment: effects on water quality and primary production. Aquacult. Env. Interac. 6, 151–174.
Salama, N.K.G., Murray, A.G., 2011. Farm size as a factor in hydrodynamic transmission of pathogens in aquaculture fish production. Aquacult. Env. Interac. 2, 61–74.
Samsing, F., Solstorm, D., Oppedal, F., Solstorm, F., Dempster, T., 2015. Gone with the flow: current velocities mediate parasitic infestation of an aquatic host. Int. J. Parasitol. 45, 559–565.
Sandwell, D.T., Gille, S., Smith, W.H., 2002. Bathymetry from space: oceanography, geophysics, and climate. Oceanogr. Geophys. Clim. 24.
Shchepetkin, A.F., McWilliams, J.C., 2005. The regional oceanic modeling system (ROMS): a split-explicit, free-surface, topography-following-coordinate oceanic model. Ocean Model 9, 347–404. http://dx.doi.org/10.1016/j.ocemod.2004.08.002.
Terray, E.A., Brumley, B.H., Strong, B., 1999. Measuring Waves and Currents With an Upward-looking ADCP.
Tironi, A., Marin, V.H., Campuzano, F.J., 2010. A management tool for assessing aquaculture environmental impacts in Chilean Patagonian Fjords: integrating hydrodynamic and pellets dispersion models. Environ. Manag. 45, 953–962.
Tsukrov, I.I., Ozbay, M., Swift, M.R., Celikkol, B., Fredriksson, D.W., Baldwin, K., 2000. Open ocean aquaculture engineering: numerical modeling. Mar. Technol. Soc. J. 34, 29–40. http://dx.doi.org/10.4031/MTSJ.34.1.4.
Tsukrov, I., Drach, A., Decew, J., Robinson Swift, M., Celikkol, B., 2011. Characterization of geometry and normal drag coefficients of copper nets. Ocean Eng. 38, 1979–1988. http://dx.doi.org/10.1016/j.oceaneng.2011.09.019.
Venayagamoorthy, S.K., Ku, H., Fringer, O.B., Chiu, A., Naylor, R.L., Koseff, J.R., 2011. Numerical modeling of aquaculture dissolved waste transport in a coastal embayment. Environ. Fluid Mech. 11, 329–352. http://dx.doi.org/10.1007/s10652-011-9209-0.
Wang, X., Olsen, L.M., Reitan, K.I., Olsen, Y., 2012. Discharge of nutrient wastes from salmon farms: environmental effects, and potential for integrated multi-trophic. Aquacult. Env. Interac. 2, 267–283.
Wekerle, C., Wang, Q., Danilov, S., Jung, T., Schröter, J., 2013. The Canadian Arctic Archipelago through flow in a multiresolution global model: model assessment and the driving mechanism of interannual variability. J. Geophys. Res. Ocean. 118, 4525–4541. http://dx.doi.org/10.1002/jgrc.20330.
Winthereig-Rasmussen, H., Simonsen, K., Patursson, Oystein, 2016. Flow through fish farming sea cages: comparing computational fluid dynamics simulations with scaled and full-scale experimental data. Ocean Eng. 124, 21–31. http://dx.doi.org/10.1016/j.oceaneng.2016.07.027.
Wunsch, C., Heimbach, P., Ponte, R., Fukumori, I., 2009. The global general circulation of the ocean estimated by the ECCO-consortium. Oceanography 22, 88–103. http://dx.doi.org/10.5670/oceanog.2009.41.
Yamada, T., Koike, K., 2011. Downscaling mesoscale meteorological models for computational wind engineering applications. J. Wind Eng. Ind. Aerodyn. 99, 199–216. http://dx.doi.org/10.1016/j.jweia.2011.01.024.
Zhao, Y.-P., Li, Y.-C., Dong, G.-H., Gui, F.-K., Teng, B., 2007. Numerical simulation of the effects of structure size ratio and mesh type on three-dimensional deformation of the fishing-net gravity cage in current. Aquac. Eng. 36, 285–301. http://dx.doi.org/10.1016/j.aquaeng.2007.01.003.
Zhao, Y.P., Bi, C.W., Dong, G.H., Gui, F.K., Cui, Y., Xu, T.J., 2013. Numerical simulation of the flow field inside and around gravity cages. Aquac. Eng. 52, 1–13. http://dx.doi.org/10.1016/j.aquaeng.2012.06.001.